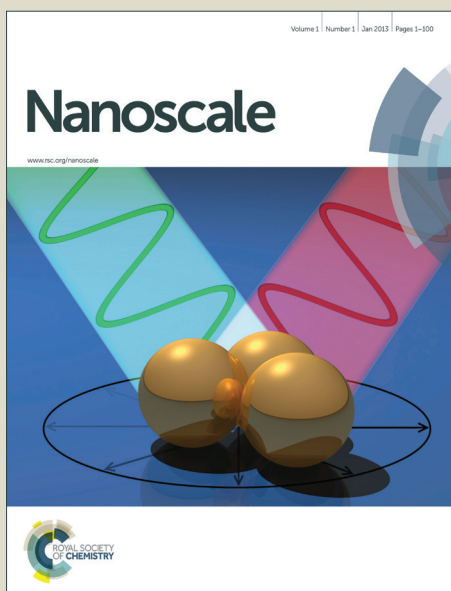


Nanoscale

Accepted Manuscript



This is an *Accepted Manuscript*, which has been through the Royal Society of Chemistry peer review process and has been accepted for publication.

Accepted Manuscripts are published online shortly after acceptance, before technical editing, formatting and proof reading. Using this free service, authors can make their results available to the community, in citable form, before we publish the edited article. We will replace this *Accepted Manuscript* with the edited and formatted *Advance Article* as soon as it is available.

You can find more information about *Accepted Manuscripts* in the [Information for Authors](#).

Please note that technical editing may introduce minor changes to the text and/or graphics, which may alter content. The journal's standard [Terms & Conditions](#) and the [Ethical guidelines](#) still apply. In no event shall the Royal Society of Chemistry be held responsible for any errors or omissions in this *Accepted Manuscript* or any consequences arising from the use of any information it contains.



Journal Name

ARTICLE

Chloride Promoted Room Temperature Preparation of Silver Nanoparticles on Two Dimensional Tungsten Oxide Nanoarchitectures for the Catalytic of Oxidation of Tertiary N-compounds to N-oxides

Received 00th January 20xx,
Accepted 00th January 20xx

DOI: 10.1039/x0xx00000x

www.rsc.org/

Shilpi Ghosh, Shankha S. Acharyya, Malika Kumar and Rajaram Bal*

Halide ions promoted two dimensional silver tungsten-based nanomaterial was synthesized by a facile one-pot synthesis protocol at room temperature. The 2D morphology features high activity and selectivity for oxidation of a wide range of tertiary N-compounds to their corresponding N-oxides. The morphology of the Ag/WO₃ materials can be varied by changing the synthesis parameters. The unique 2D plate like morphology of tungsten oxide increases adsorption sites of the support, leading to less sintering and higher dispersion of silver nanoparticles, resulting to the significantly enhanced activity for reaction. The influence of reaction parameters such as temperature, substrate to oxidant molar ratio, reaction time, etc. were investigated in detail. The catalyst was characterized by XRD, XPS, ICP-AES, TGA, FT-IR, UV-vis, RAMAN, SEM, TEM and STEM. Raman studies further provide mechanistic insight which proves the formation of peroxo tungsten species is responsible for N-oxidation reaction. A high stability and recyclability of the 2D Ag/WO₃ nanoplates is also observed under the investigated conditions.

1. Introduction

Two-dimensional (2D) nanostructures have garnered a tremendous amount of interest in recent years because they exhibit a range of fascinating electronic, catalytic, and optical properties that largely differ from conventional bulk, zero- and one-dimensional nanocrystal counterparts.¹⁻³ While freestanding planar configuration is often desirable, a range of applications such as catalysis and sensing benefit greatly from the accessibility to large surface areas. During the past two decades, investigations have been carried out to explore efficient routes for the size and shape controlled synthesis of inorganic nanocrystals. Since ways of making graphene were devised,⁴ there have been significant research efforts to synthesize 2D nanocrystals of various materials, including metals,⁵ oxides,⁶ and chalcogenides.⁷ For the successful preparation of the 2D layered nanostructures, the appropriate choice of reactants and growth conditions is critical to ensure kinetically controlled pathways that keep the intrinsic anisotropic planar growth of 2D nanostructures. The catalytic efficiency of nanostructures is primarily governed by the size and shape of the nanocrystals and the composition of the metals and support used.⁸ The control over both the dispersion and the particle size distribution of supported metal nanoparticles used in

heterogeneous catalysts is of paramount importance. Novel metal nanoparticles such as silver have especially been of interest owing to their interesting size dependent properties in various reactions.⁹⁻¹¹ Of late, supported silver nanocatalysts have found to be very effective catalyst for oxidation reactions.¹² Significant research efforts have been made for the synthesis of silver nanoparticles on different transitional and non-transitional metal supports such as titania, alumina, silica etc.¹³⁻¹⁶ The methods associated for the synthesis of supported Ag nanoparticles such as sonochemical, microwave irradiation, vapour deposition etc. need drastic conditions like high temperature, hydrothermal treatment, use of solvents, which make the whole process not only environmentally unfriendly but also highly energy-intensive.¹⁷⁻²⁰ Owing to these, considerable research efforts have been made to prepare supported Ag nanostructured materials in solution phase.

Herein, we report for the first time room temperature fabrication of highly dispersed very small AgNPs on 2D WO₃ nanoplates for the oxidation of aromatic tertiary amines to their corresponding N-oxides with hydrogen peroxide as oxidant with very high yield under mild conditions. While significant research efforts have focused on new 2D materials ranging from graphene to layered chalcogenides such as WS₂, MoS₂, or Bi₂Se₃, Si₂Te₃ seems an obvious choice for bringing unique material properties into the realm of integrated electronic and optical applications, the room temperature fabrication of silver nanoparticles on 2D WO₃ nanoplates and their catalytic applications have not been investigated till date.^{4,7} In comparison with the spherical nanoparticles, a firm understanding of the growth parameters and reactions conditions that yield 2D plate or sheetlike nanostructures is at the present time not well established. Generally, gas-phase synthetic protocols, such as the vapor-liquid-solid (VLS), thermal evaporation methods, sonochemical and ultrasonic spray pyrolysis methods and hot

Catalytic Conversion & Processes Division, CSIR-Indian Institute of Petroleum, Dehradun 248005, India

Corresponding author. Tel.: +91 135 2525797; Fax: +91 135 2660202

E-mail addresses: raja@iip.res.in

Electronic Supplementary Information (ESI) available: [details of any supplementary information available should be included here]. See

DOI: 10.1039/x0xx00000x

injection method have been employed for the synthesis of two dimensional nanostructures, which are all energy intrinsic processes: require harsh condition, such as high temperature, use of solvents, costly and tedious reaction set-up.²¹ Many of the 2D nanocrystals have been generated from exfoliation of materials with layered structures, and tiny amounts of products are generally produced.²²

We show in this work that the presence of halides can also play a pivotal role in facilitating the platelike growth of tungsten oxide nanostructures, and the dimensionality of the synthesized nanostructure can be tuned from 0D to 2D by simply varying the reaction condition. Insofar, AgW is concerned; our previous reports deal with the synthesis of spherical nanoparticles, 1D nanorods, 3D hierarchical superstructures by one pot synthesis method.²³⁻²⁵ But synthesis of 2D Ag/WO₃ nanoplates and their catalytic applications have not been explored.

Oxidation reactions are the most fundamental reaction in organic chemistry. N-oxidation of heterocyclic tertiary amines has long been a topic of substantial interest owing to the usefulness of heterocyclic N-oxides in the field of chemistry as highly valuable synthetic intermediates and also for their biological importance.²⁶⁻²⁸ Heterocyclic N-oxides used as protecting groups, auxiliary agents, oxidants, ligands in metal complexes.²⁹⁻³² N-oxides offer functional group manipulation and structural modification possibilities that are not accessible for other methods.³³ Various substituted pyridines and their derivatives, generally used as a building block for biologically active compounds and materials, are produced from pyridine N-oxides. Amine N-oxides are also vital components for ubiquitously used materials such as toilet soaps, toothpastes, detergent powders, shampoos and cosmetics as well as in biomedical applications.³⁴⁻³⁶ Several oxidants have been used for selective transformation, but most of the methods suffer from the use of stoichiometric amounts of corrosive acids or toxic metallic compounds and generate undesirable waste.³⁷⁻⁴¹ N-oxides production have been achieved by various oxidizing agents, which includes peracetic acid, m-CPBA,³² dioxiranes,⁴³ caro's acid,⁴⁴ sodium perborate in acetic acid.⁴⁵ But the use of such oxidants is not environmentally friendly due to the generation of substantial amount of effluent during the reaction process and also require a laborious work-up procedure. Thus, the exploration of a true heterogeneous catalyst with ease of separability and recyclability for the production of N-oxides using environmentally benign oxidizing agent H₂O₂, is highly demanding. H₂O₂ based oxidation is of great advantage to the environment and industry because it generates H₂O as the by-product, it has the high content of active oxygen species (47 wt%).⁴⁶ Moreover, H₂O₂ is cheaper and safer to use than the other peroxides and peracids. Recently, ruthenium based catalyst is well known for catalyzing heterocyclic amines to their corresponding N-oxides.⁴⁷ But the high cost of ruthenium is a major drawback of this process. K₆[PW₉V₃O₄₀] has been reported for the oxidation of pyridine with 84% yield.⁴⁸ Similarly, methyltrioxorhenium,⁴⁹ manganese porphyrin,⁵⁰ flavin,⁵¹ tungsten sulfide,⁵² tungsten-based polyperoxometalates,⁵³ selenium⁵⁴ oxides, silica supported vanadium catalyst,⁵⁵ 2,2,2-trifluoroacetophenone,⁵⁶ silica immobilized perfluoroketone,⁵⁷ have been shown to catalyze the N-oxidation of tertiary amines in the presence of aqueous H₂O₂. But the catalyst preparation methods involve multistep processes, require harsh synthesis conditions.

Herein, in the present work, we report for the first time room temperature facile synthesis of highly dispersed very small AgNPs

(2-5 nm) on 2D WO₃ nanoplates for the oxidation of tertiary N-compounds to their corresponding N-oxides with hydrogen peroxide as oxidant with very high yield. Our previously reported silver tungsten nanoparticle catalyst selectively converted aromatic primary amine, such as aniline to azoxybenzene with high yield,²³ but the AgW nanoparticles exhibit poor catalytic performance for N-oxidation reaction as compared to that of the AgW 2D nanoplate morphology. It is also well known fact that we know that the catalytic efficiency of nanostructures is primarily governed by the size and shape of the nanocrystals. The open 2D structure of tungsten oxide nanoplates increases adsorption sites of the support leading to less sintering and higher dispersion of silver nanoparticles; moreover the presence of 2D nanoplates influences the interactions between the reactants and catalyst surface during the reaction which may be attributed to the enhanced catalytic performance. Here, the controlled growth of Ag NPs on 2D WO₃ with efficient oxidative property opens up opportunities for new applications in catalysis chemistry.

The significant features of our synthesis are as follows: a) the synthesis is based on simple one pot chemical route at room temperature condition, b) first large scale tunable production of Ag/WO₃ 2D nanoplate, c) freestanding layered WO₃ provides wider accessibility to large surface areas, d) the platelike morphology is highly reproducible and large quantity (~15 g) material can be prepared, e) avoids using harsh condition such as: hydrothermal treatment and hot injection method which generally employ high temperature synthesis process and finally f) the material is highly stable and exhibit good recyclability after catalytic reactions.

2. Experimental

2.1. Materials

H₂WO₄, AgCl, cetyltrimethylammonium bromide, HPLC grade (~99.9%) pyridine, 3-picoline, acetonitrile etc. were purchased from Sigma-Aldrich Co. Hydrogen Peroxide (50 wt % in water) was purchased from Merck KGaA, Darmstadt, Germany. All the chemicals were used without further purification. Double distilled water was used during the preparation of catalyst.

2.2. Synthetic procedures

The Ag/WO₃ plate-like nanocatalyst was prepared by surfactant assisted method modifying our own preparation method.²³⁻²⁵ Aqueous solution of silver nitrate (0.6 g) was added to vigorous stirred 9.3 g tungstic acid dissolved in deionized water. An aqueous solution of CTAB (1.5 g) was added drop wise to the reaction mixture. The pH of the medium was adjusted to ~3 by dropwise addition of HCl. The reagents were added maintaining the molar ratio Ag: CTAB = 1: 1. After stirring for 5 h, the so obtained homogeneous solution was washed with ethanol and dried at 110 °C, for 10 h, followed by calcination at a very slow ramping of 0.5°C/min. at 400 °C for 6 h in air.

2.3. Catalyst characterization techniques

A thorough characterization of the catalyst was done using different characterization techniques like XRD, ICP-AES, SEM, TEM, BET surface area, EXAFS, XPS and TGA. Powder X-ray diffraction patterns were collected on a Bruker D8 advance X-ray diffractometer fitted with a Lynx eye high-speed strip detector and a Cu K_α radiation

source. Diffraction patterns in the 2° - 80° region were recorded at a rate of 0.5 degrees (2θ) per minute. Scanning electron microscopy (SEM) images were taken on a FEI Quanta 200 F, using tungsten filament doped with lanthanumhexaboride (LaB_6) as an X-ray source, fitted with an ETD detector with high vacuum mode using secondary electrons and an acceleration tension of 10 or 30 kV. Samples were analyzed by spreading them on a carbon tape. Energy dispersive X-ray spectroscopy (EDX) was used in connection with SEM for the elemental analysis. The elemental mapping was also collected with the same spectrophotometer. TEM images were collected using a JEOL JEM 2100 microscope, and samples were prepared by mounting an ethanol-dispersed sample on a lacey carbon formvar coated Cu grid. X-Ray photoelectron spectra were recorded on a Thermo Scientific K-Alpha X-Ray photoelectron spectrometer and binding energies (± 0.1 eV) were determined with respect to the position C 1s peak at 284.8 eV. Raman spectra were measured by a microscopic Raman spectroscopic system, Renishaw Ramascope, excited with a He-Ne Laser at 633 nm. Chemical analyses of the metallic constituents were carried out by Inductively Coupled Plasma Atomic Emission Spectrometer; model: PS 3000 uv, (DRE), Leeman Labs, Inc, (USA). Fourier Transformation Infra-red Spectroscopy (FTIR) spectra were recorded on a Thermo Nicolet 8700 (USA) instrument with the operating conditions: resolution: 4cm^{-1} , scan: 36, operating temperature: $23\text{-}25^{\circ}\text{C}$ and the frequency range $4000\text{-}400\text{ cm}^{-1}$. Thermogravimetric Analyses (TGA) of the uncalcined catalyst were carried out in a Pyris Diamond, Perkin Elmer instruments, and technology by SII (Seiko Instruments Inc), USA] instrument-balance by heating 2.15 mg samples at $5^{\circ}\text{C min}^{-1}$ in flowing nitrogen.

2.4. Catalytic reaction

The N-oxidation of tertiary N-compounds with H_2O_2 (50%) was carried out in a 50 ml round bottomed flask equipped with refluxed condenser. The reaction mixture contains 0.1 g of catalyst, 10 ml acetonitrile, 1.0 g substrate, substrate: H_2O_2 in the mole ratio of 1:3. Small aliquots of the sample were withdrawn from the reaction mixture at regular interval of time for analysis. At the end of the reaction, the catalyst was separated from the reaction mixture by centrifugation and washed well with diethyl ether followed by drying in an oven at 80°C for 2 h and was reused for the subsequent N-oxidation of tertiary N-compounds. The centrifugate was dried over anhydrous MgSO_4 to afford the product which was purified by passing through a column of silica gel using dichloromethane-methanol (90 : 10) as an eluent. The products (N-oxides) were identified by NMR and GC-MS analysis. The products were analysed by Gas Chromatography (GC, Agilent 7890) connected with a HP5 capillary column and flame ionization detector (FID) and identified by GCMS using supelco Equity 1 column (30 m length, .25 mm i.d.) and $^1\text{H-NMR}$. The individual yields were calculated and normalized with respect to the GC response factors. The C- balance as well as material balance was carried out for most of the experiments and it was found between 98-102%.

The conversion of tertiary amines and the selectivity of the products in the reaction are calculated as:

Substrate conversion (%) = $\left[\frac{\text{Substrate converted (mole)}}{\text{substrate used (mole)}} \times 100\right]$,

Product selectivity = $\left[\frac{\text{Product conversion (mole)}}{\text{substrate used (mole)}} \times 100\right]$.

3. Results and discussion

3.1. Generation of Silver-tungsten nanoplates

The Ag/WO_3 nanoplate catalyst was synthesized by modifying our own preparation method²³⁻²⁵ taking tungstic acid and silver nitrate as the precursors of W and Ag respectively and cetyltrimethylammonium bromide (CTAB) as a surfactant. The pH of the medium was maintained ~ 3 by adding HCl. The reagents were added maintaining the molar ratio Ag: CTAB = 1:1. CTAB is a cationic surfactant that plays an important role in controlling the micro and nano architectures under template effect. The growth of the certain architecture is associated with the selective interaction of the organic surfactants on certain crystallographic facets to stimulate the crystal growth.

The growth evolution of the nanoplates as a function of time was investigated by taking aliquots at different stages of the reaction and characterizing via SEM. At an early stage of the reaction after 1 hr stirring, we could observe combination of aggregated nanoplates and nanoparticles, indicating the fact that, the plates grew slowly at the expense of these aggregated particles (Fig. S1). Well separated 2D nanoplates were obtained after 3-5 h stirring time (Fig.3). Further increasing stirring time (10 h), nanoplates were self assembled and form agglomerated morphology (Fig. S2). Previously our synthesis processes involve the use of tungstic acid and silver nitrate as precursors in a basic solution which could produce 1D rodlike morphology (Fig. S3).²⁴ The apparent differences between the synthesis processes confirm the effect of preparation conditions on the catalyst morphology. The effect of the Cl^- ions on the growth of the tungsten oxide nanoplates was investigated. Without addition of Cl^- ion, spherical particles as shown in Fig. S4 were observed. So we can affirm that Cl^- has a definite role towards the formation of plate-like structure. It is worthwhile to mention that when we added silver nitrate as Ag precursor and maintained $\text{pH} \sim 3$, by using HF, similar plate like morphology was obtained (Fig. S5). Indeed, the use of AgCl as the silver precursor also gives essentially identical results in terms of nanostructures and intermediates produced. So we can affirm that Cl^- has a definite role towards the formation of plate-like structure. Namely, that the formation of nanoplate is favoured at high Ag: CTAB=1:1(Fig. 3). In a control experiment, fixing the reaction at room temperature and keeping all other parameters constant, without the addition of surfactant CTAB, only irregularly aggregated nanoplates were obtained (Fig. S6). When the synthesis was performed taking high concentration of CTAB, with Ag:CTAB=1:5, agglomerated structure was formed (Fig. S7). Also low concentration of CTAB (Ag:CTAB= 1:0.5) was not favourable for the growth of 2D nanoplate (Fig. S8). This indicates that CTAB could induce and greatly enhance the directing role of chlorides in the preparation of tungsten oxide 2D nanoplates. In our experiment, it is supposed that chloride ions first coordinated with H_2WO_4 through hydrogen bonding between hydrogen atoms of tungstic acid and Cl^- ions and induce oriented attachment on the planes of tungstic acid. Cetyltrimethyl ammonium bromide (CTAB), being a cationic surfactant, ionized in aqueous solution forming CTA^+ . The positively charged CTA^+ is supposed to stabilize the $[\text{HO-W}(=\text{O})_2\text{-OH} \cdots \text{Cl}^-]$ species through electrostatic interaction between CTA^+ and Cl^- ions. This CTA^+ stabilized H_2WO_4 moiety acts as a template and fosters lateral growth. This is in agreement with the previous reports where F^- ions induce platelike morphology.⁵⁸ Also,

the chloride ions might enhance the repulsion between the organic layers of bulky CTAB and inhibit the fusion of nanoplates, resulting in weakened interactions between the nanoplates and well-separated 2D nanoplates are formed. We have performed SEM-EDAX analysis of the Ag/WO₃ sample in the mid of catalyst preparation process to check the presence of chlorine, which shows the presence of Cl (chlorine) along with C, N, Br, Ag, W, O (Fig. S9). After repeated washing the sample, the chloride ions washed away and we did not observe chlorine in the before calcination sample, Fig. S10., we observed only Ag, W, O, C, N. XPS survey spectrum of the before calcination sample showed the presence of carbon and nitrogen along with Ag, W, O (Fig. S11); since during washing the complete removal of cationic surfactant CTAB did not take place. As chlorine washed away during filtration, we did not observe any XPS peaks for Cl. We would like to mention here that the intensity of the N spectra is low and we believe that some of the CTAB groups are present in the bulk, not on the surface. But, after calcination sample showed only the presence of Ag, W and O in the XPS spectra as removal of CTAB occurs during calcinations (Fig. 2). Our XRD and XPS studies after calcination reveal the presence of silver nanoparticles Ag(0) and TEM images proves all these Ag NPs are uniformly distributed on the surface of WO₃ nanoplates. This study further demonstrates that the top surfaces of the WO₃ nanoplates remain passivated by chemically saturated Ag atoms. Therefore, lateral dimension increases much faster than the vertical thickness. We can say that the combination of Cl⁻ and Ag can efficiently passivate growth along the vertical direction and facilitate the formation of 2D nanoplates. It is pertinent to mention that Cl⁻ ions influence the silver underpotential deposition (UPD) at the nanoplates surface.⁵⁹ The results described in this work collectively exemplify the use of halides in promoting lateral growth in tungsten oxide nanostructures, and adds to the growing synthetic toolkit for producing two dimensional nanomaterials.

There is also possibility that since H₂WO₄ is known to consist of layers of [WO₆] octahedra, H₂WO₄ can provide further impetus for plate formation.⁶⁰ It is believed that the inherent growth habit of the crystals as well as the specific interaction between the chlorides and the crystal surfaces may have played an important role in control the morphology of the final crystals.

3.2. Catalyst characterization

The amount of silver present in the Ag/WO₃ platelike nanocatalyst, estimated by ICP-AES, was found to be 4.2 wt%. The related X-ray diffraction (XRD) pattern of the Ag/WO₃ nanostructured catalyst showed the peaks at 2θ values of 23.1°, 23.6°, 24.4°, 33.3° and 34.1°, confirm the formation of monoclinic WO₃ (JCPDS No. 43-1035, space group: P2₁/n) (Fig.1). In addition, four diffraction peaks at 2θ values of 38.2, 44.2, 64.3 and 77.4° corresponding to the metallic Ag crystal faces of (111), (200), (220) and (311) respectively, which coincide well with the literature values (JCPDS No. 04-0783). After catalysis, the metallic state of silver remained intact (Fig. 1e). We found that the intensity of the Ag reflection peaks of Ag/WO₃ nanoplates are less, suggesting a smaller silver particle size and a higher dispersion of silver nanoparticles over tungsten oxide nanoplates. The X-ray photoelectron spectroscopy (XPS) survey spectrum of the fresh sample (after calcination) proves the presence of Ag, W and O (Fig. 2a). The peaks XPS analyses clearly the presence of metallic silver in the fresh sample from the corresponding Ag 3d_{5/2} and Ag 3d_{3/2} binding energy values of 368.3 eV and 374.1 eV respectively (Fig. 2b).²³ The W 4f_{5/2} and 4f_{7/2} spectra attributed to the binding energies 37.9 eV and 35.8 eV

respectively suggesting that the tungsten in the tungsten oxide sample exists as W⁺⁶.²³ (Fig. 2c) The O1s spectrum exhibited peak at binding energy 530.6 eV, which can be attributed to the oxygen bounded to W⁺⁶ i.e. WO₃ (Fig. 2d). The corresponding Ag 3d binding energy of the spent catalyst ~368.3 eV, confirms that the oxidation state of metallic silver does not change during catalysis which accords well to the XRD results of the spent catalyst (Fig. S12). To investigate the morphology of the obtained silver-tungsten catalyst, the SEM and TEM images were measured. SEM images of the catalyst show a hierarchical morphology, which consists of numerous regular and interconnected nanoplates which exhibit nanometer-sized thickness (Fig. 3). A sideview of the High resolution Transmission Electron Microscopy (HRTEM) image exhibits that the entire nanoplate was covered by densely populated very small silver nanoparticles of ~2-5 nm (Fig.4b). The corresponding TEM histogram of Ag nanoparticles showed a very narrow particle size distribution with sizes between 2-5 nm (Fig 4b, inset). The lattice fringe distance of 0.38 nm indicates the [020] lattice spacing of WO₃ and the distance of 0.23 nm corresponds to [111] plane of Ag (Fig. 4c). The TEM elemental mapping indicates the presence of Ag, W and O species and further ascertains the uniform dispersion of AgNPs on tungsten oxide support, which ensures intimate contact between silver and tungsten oxide (Fig. 5). The TEM electron diffraction (ED) pattern showed only the presence of silver, oxygen and tungsten and no impurities could be observed in the spectra (Fig. S13). The TEM image of the spent catalyst reveals that the nanoplate structure of AgW is well retained after catalysis and there was almost no change in the sizes of silver nanoparticles after N-oxidation (Fig. 4d). The embedment of CTAB molecules on the uncalcined catalyst was further confirmed from the FTIR analysis (Fig. 6). The peaks of the sample at 812, 1067 cm⁻¹ can be assigned to the C-N⁺ stretching modes of CTAB molecules. The peaks at 1379 and at 1402 cm⁻¹ are assigned to symmetric mode of vibration of the head groups of the methylene moiety (N⁺-CH₃) and CH₂ scissoring mode respectively.⁶¹ The frequencies above 1600 cm⁻¹ to 3000 cm⁻¹ are due to CH₂ symmetric and anti symmetric vibrations, respectively. It is to be noted that, the shift of vibrations to lower frequency occurred as the alkyl chains experienced a more hydrophobic environment in Ag-W blocks upon the surface of which the CTA-moieties were supposed to be bound. It can be inferred that, the mutual interactions between CTAB and the Ag-W surface have taken place. These typical frequencies were absent when the material was calcined at 400 °C in air (fresh catalyst) in the case of the prepared catalyst, which indicated that, the embedded CTAB moieties have been completely removed from the catalyst surface during calcination. In the crystalline structure of WO₃, W atoms are located in the centre of WO₆ octahedra with O at the vertices forming W-O-W connections.⁶⁰ For such an arrangement, the IR active bands are fundamental vibrations of W=O, W-O and W-O-W. These can be stretching (u) or in-plane bending vibrations (δ) and out-of-plane wagging (γ).⁶⁰ The main WO₃ vibrations are found in the 1700–380 cm⁻¹ IR region. All synthesis temperatures present characteristic peaks at 567, 784, 893, 964, 1399 cm⁻¹ associated with γ(W-O-W), u(W-O-W), u(W-O-W), u(W-O, W=O), u(OH) in W-OH respectively. The embedment of CTAB molecules on the pre-calcined catalyst surface was further confirmed from TGA analysis (Fig.7). TGA analysis was operated to understand the various decomposition regimes as shown in Fig. 9. The TGA diagram showed that the weight loss around 286 °C is assigned to the decomposition of CTA moiety. Further weight loss was not observed when the temperature was further increased from 400°-700° C, indicating the stability of the catalyst upto 700° C.

Total mass reduction of ~17.5% confirmed the complete removal of the surfactant CTAB. Further weight loss was not observed when the temperature was further increased from 400 to 700 °C, no weight loss speculated, indicating the formation of stable Ag/WO₃ catalyst in that temperature zone. Fig. 8 compares the diffuse reflectance UV-vis spectra for pure WO₃ and Ag/WO₃ nanoplates. The absorption edge for pure WO₃ is located at 473 nm, whereas, for the Ag/WO₃ nanoplates a comparatively larger shift (red shift) in the absorption edge is observed at 503 nm. Thus, Ag/WO₃ nanoplates can absorb solar energy over a broad range in the visible region as compared to the pure tungsten oxide. Thus nanoplate like morphology exhibits localized surface plasmon resonance effect (LSPR) due to the presence of very small silver nanoparticles (3-5 nm) on tungsten oxide nanoplates.⁶² Raman spectra of the Ag/WO₃ nanostructure catalyst is characterized by well resolved sharp bands (Fig. 9). The high intense band at 800 cm⁻¹ in the Raman spectrum corresponds to the symmetric stretching vibration and the intense band at 711 cm⁻¹ corresponds to the asymmetric stretching vibration of O-W-O bond.²⁵ The medium intense band at 260 cm⁻¹ and weak band at 323 cm⁻¹ are due to the bending vibrations of O-W-O bond. The treatment of Ag/WO₃ with H₂O₂ resulted in new absorption band at 571 and 873 cm⁻¹ in the Raman spectrum (Fig. 9 b). This band could be assigned as $\nu(\text{W}(\text{O}_2))_{\text{asym}}$ and $\nu(\text{O}-\text{O})$ respectively, which demonstrated that peroxy species was formed in presence of H₂O₂.⁶³ This role is clearly evidenced by the fact that when we recovered and dried the catalysts after H₂O₂ addition the peroxy signal remained. After subsequent pyridine addition, the peroxy signal disappeared, thus proving the reaction of pyridine with this surface-bound peroxy species (Fig. 10c). The Raman spectra of the catalyst before use and after recovery from the reaction was not significantly different reflects the structural stability of the catalyst under the reaction condition.

3.3. Catalytic activity of Ag/WO₃ nanoplate catalyst

Ag/WO₃ nanostructured catalyst was tested as a heterogeneous catalyst for N-oxidation of heterocyclic tertiary amines with aqueous H₂O₂ at atmospheric pressure at 80°C temperature in presence of acetonitrile solvent. The activities of the catalysts are shown in Table 1. The heterocyclic tertiary amines were found to be very active for selective transformation to their corresponding N-oxides using 10 wt% of catalyst (w.r.t. substrate) and substrate:H₂O₂ molar ratio of 1:3. Pyridine and its substituents such as: 3-methyl pyridine, 3-chloro pyridine, quinoline were selectively transformed to their corresponding N-oxides (Table 1, entries 1-4), even phenazine, pyrazine, quinoxaline were also transformed to their N-oxides very selectively (Table 1, entries 5-7). Different alkyl amines and its substituents, such as triphenyl amine, N, N-dimethyl aniline, N-butyl dimethyl amine, quinuclidine, N, N-dimethyl-o-toluidine (meta and para also), etc. selectively transformed to their corresponding n-oxides very selectively (Table 1, entries 8-15). It is worthwhile to mention that the comparatively lesser selectivity towards N-oxides for N, N-dimethyl toluidine series due cracked products (Table 1, entries 9, 13-12). The catalytic activity of the Ag/WO₃ nanostructured catalyst was studied using pyridine as a model compound. A series of controlled catalytic experiments using Ag/WO₃ nanostructured catalyst were carried out to understand the variation of pyridine to pyridine N-oxide conversion as a function of time, temperature and pyridine to H₂O₂ mole ratio. The catalyst exhibits a pyridine conversion of 88% with 99% selectivity to pyridine N-oxide at 80 °C. The effect of temperature with pyridine

conversion was studied and it was found that at room temperature, the catalyst exhibits 20% conversion with 99% N-oxide selectivity (Fig. 10). With increasing temperature, the conversion increases keeping the selectivity constant at 99%. 80°C temperature was found to be the optimum one, since further increase in temperature to 110°C, the conversion decreases to 79%, most probably due to the decomposition of H₂O₂ at high temperature. However, the selectivity of N-oxide was kept constant throughout the temperature variation. The substrate: H₂O₂ mole ratio was also varied (Fig. 11). In fact, when, pyridine: H₂O₂ mole ratio was adjusted to 1:1, the yield was very low (~34.6%) and upon increasing the substrate: H₂O₂ mole ratio to 1:3, the conversion increases significantly to 88 % with 99% N-oxide selectivity. Further increase substrate: H₂O₂ mole ratio to 1:5, the conversion did not increase significantly (from 88% to 90%), further increase in the mole ratio to 1:10, the conversion decreased significantly to 76%; this phenomenon can be attributed to the fact that since water is produced in the medium due to the decomposition of hydrogen peroxide, which hinders the reactant molecules to come in close contact with the catalyst.

It has to be noted that the amines containing two nitrogen atoms such as: quinoxaline, pyrazine, phenazine were also selectively transformed to their corresponding single N-oxides very selectively (99%), without forming N, N-di oxides at a substrate: H₂O₂ mole ratio of 1:3 (Table 1, entries 5,-7). We also observed that further increase in the mole ratio to 1:5, no N, N-dioxides were formed. When the mole ratio was kept at 1:10, lower conversion was observed. This may be attributed to the fact that all these planar (sp² hybridization) N-containing substrates interact with the plate-like catalyst surface in a perpendicular fashion through the interaction between N-atom and the catalyst surface, which favour one sided attack of the oxygen atom to the nitrogen atom of pyridine. We also observed an increasing trend in pyridine conversion with time keeping the selectivity to N-oxide constant at 99% (Fig. 12). After 6 h reaction, the catalyst exhibited 27% conversion, the conversion increases to 88% after 24 h and after that with prolonged time the conversion was almost constant. The oxidation reaction barely proceeded in the absence of the catalyst (Table 2, entry 14). The main purpose of nanoparticle catalysis lies with activity promotion and selectivity enhancement leaving aside bulk material. It has to be noted that Ag/WO₃ catalyst prepared by the conventional impregnation method exhibited much lesser activity due to the larger particle size and irregular shape and low specific surface area (Table 2, entry 5) (Fig. S14). The conventional catalyst also showed maximum leaching tendency. So, particles in the nano regime definitely have a role towards the higher catalytic efficiency. Furthermore, Ag/WO₃ nanostructured catalyst exhibited greater H₂O₂ efficiency as compared to alone Ag or WO₃ catalyst prepared by surfactant assisted method (Table 2, entries 3, 4). Commercial WO₃ catalyze oxidation reaction less efficiently (Table 2, entry 2), moreover severe leaching caused during reaction. Commercial silver also showed very little activity (Table 2, entry 1). Moreover, our previously reported Ag/WO₃ nanoparticles exhibited poor catalytic activity (Table 2, Entry 8). The unique nanoplate morphology of tungsten oxide increases adsorption sites of the support, leading to less sintering and higher dispersion of silver nanoparticles, resulting to the significantly enhanced activity for reaction. The open structure of the 2D WO₃ nanoplates allows easy access of the oxidant and reactant molecules, as a result larger activity could be expected. Additionally, in order to investigate the effect of support on catalytic performance, we prepare a series of

comparable catalysts on several other supports, including Cr_2O_3 , MoO_3 , TiO_2 (Table 2, entries 11-13). All of these catalysts were evaluated for the N-oxidation reaction, with the results listed in Table 2. Generally most catalysts exhibited a much lower N-oxide conversion, indicating that WO_3 is an effective support of the silver catalyst for N-oxidation reaction.

Based on our experiments, it is proposed that strong metal support interactions exist between Ag NPs and WO_3 nanoplates. In order to verify the proposal, the HRTEM results showed clear Ag- WO_3 interfaces (Fig. 4c). Other oxide-metal interfacial sites and the strong metal support interaction have been known for their higher activity in various reactions, such as Au-oxide and Pt-oxide.^{64,65} From the above results, it is reasonable to propose that the Ag- WO_3 interface and interactions therein play an important role in oxidation of tertiary nitrogen compounds to their corresponding N-oxides. We believe that a synergistic interaction between Ag and WO_3 in the Ag/ WO_3 plate like catalyst plays the key role for showing the higher catalytic activity. Aqueous H_2O_2 is found to be the best oxidant among the oxidants, whereas, tert-butyl hydroperoxide (TBHP) and molecular oxygen were also employed in the oxidation of tertiary amines. The oxidant TBHP gave very poor results, while the reaction employing molecular oxygen did not proceed (Table 2, entries 9, 10). Thus H_2O_2 is an ideal and environment-friendly oxidant, in terms of its price, availability and gives only water as by-product.

3.4. Reaction mechanism

The plausible reaction mechanism in the N-oxidation of tertiary amines to N-oxides as described in Scheme 1, involves the formation of a peroxy tungsten species on interaction of tungsten oxide with hydrogen peroxide. That the activation of hydrogen peroxide is taking place in presence of tungsten oxide, is also evidenced from Raman spectroscopic study. The nitrogen atom of the tertiary amine is likely to be attached to the surface of the silver nanoparticles. It is proposed that the interaction between the silver and nitrogen is due to charge transfer between N lone pair and vacant d orbital of Ag ($p\pi-d\pi$ interaction) resulting in weak N-Ag type bond at the surface of the catalyst.^{47a} The tertiary amine undergoes nucleophilic reaction with peroxy tungsten species to give corresponding N-oxide product. The rate of oxygen transfer from tungsten peroxy species ($\text{W}(\text{O}_2)_{\text{asympt}}$) to the reactant may be facilitated in presence of Ag(0) by enhancing the polarization of O-O bond of tungsten peroxy species. The results concluded that the mechanism for the N-oxidation of tertiary amines involves tungsten peroxy species, as an intermediate. This role is clearly evidenced by the fact that when we recovered and dried the catalysts after H_2O_2 addition the peroxy signal remained (Raman study). After subsequent pyridine addition, the peroxy signal disappeared, thus proving the reaction of pyridine with this surface-bound peroxy species.

3.5. Reusability of the Catalyst

We tested the reusability of the Ag/ WO_3 2D platelike nanostructure without further regeneration. The oxidation reaction was carried out with the reused catalyst under the same reaction condition. Activity of the recovered catalyst after four consecutive runs did not lead to any significant decline in its catalytic activity in terms of conversion and selectivity (Fig. 13). After completion of the

reaction, the solid catalyst was removed from the reaction mixture by filtration during hot condition and the reaction was allowed to proceed with the filtrate under the same conditions. The reaction was completely stopped after the removal of the catalyst. Another important finding is that the oxidation pathway does not involve homogeneous catalysis by dissolving tungsten or silver species. TEM image does not show any change compared to the initial morphology and particle size distribution (Fig. 4d). We also observed that after four recycles, a negligible amount of leached Ag and W were detected by ICP-AES (the concentration of both metals were <2 ppb.), which further confirms the true heterogeneity of the catalyst. XPS also confirmed that almost no change was occurred in the metallic state of the silver before and after four reuses.

4. Conclusions

In summary, we developed a new approach to the room temperature preparation of 2-5 nm silver nanoparticles supported on 2D tungsten oxide nanoplates. Halide ions play decisive roles in determining the morphology of the particles. In the light of the findings, we can say that the Ag/ WO_3 nanoplates serve as a highly selective heterogeneous catalyst for the one step selective N-oxidation of a wide range of tertiary amines to their corresponding N-oxides with H_2O_2 as oxidant with high yield. Moreover, the morphology of the nanoplates does not change at all even after four catalytic cycles. The catalyst characterization shows that Ag nanoparticles supported WO_3 nanoplate catalyst possesses higher Ag dispersion, improved metal-support interaction and synergistic interaction, leading to the significantly enhanced activity for N-oxidation reaction.

Acknowledgements

S.G. thanks UGC, S.S.A. thanks CSIR, India for the fellowship. R.B. thanks CSIR, New Delhi for the financial support in the form of 12 FYP Project (CSC-0125, CSC 0117). Director, CSIR-IIP, is acknowledged for his support and encouragement. The authors thank Analytical Section Division, CSIR-Indian Institute of Petroleum.

Notes and references

#Electronic supplementary information (ESI) available.

1. C. J. Luo, H. D. Jang and J. Huang, *ACS Nano*, 2013, **7**, 1464.
2. X. Huang, S. Tang, X. Mu, Y. Dai, G. Chen, Z. Zhou, F. Ruan, Z. Yang and N. Zheng, *Nat. Nanotechnol.*, 2011, **6**, 28.
3. L. Li, Z. Chen, Y. Hu, X. Wang, T. Zhang, W. Chen, and Q. Wang, *J. Am. Chem. Soc.*, 2013, **135**, 1213.
4. R. Si, Y.-W. Zhang, L.-P. You and C.-H. Yan, *Angew. Chem.*, 2005, **117**, 3320.
5. V. F. Puentes, D. Zanchet, C. K. Erdonmez and A. P. Alivisatos, *J. Am. Chem. Soc.*, 2002, **124**, 12874.
6. X. Li, G. Zhang, X. Bai, X. Sun, X. Wang, E. Wang and H. Dai, *Nat. Nanotechnol.*, 2008, **3**, 538.
7. C. Li, L. Huang, G. P. Snigdha, Y. Yu, L. and Cao, *ACS Nano*, 2012, **6**, 8868.

- 8.S. J. Tauster, S. C. Fung and R. L. Garten, *J. Am. Chem. Soc.*, 1978, **100**,170.
- 9.Z. Qu, M. Cheng, W. Huang and X. J. Bao. *J. Catal.*, 2005, **229**,446.
- 10.R. A. Van Santen and H. P. C. E. Kuipers, *Adv. Catal.*, 1987, **35**, 265.
- 11.J. Lu, J. J. Bravo-Suárez, A. Takahashi, M. Haruta, S. T. Oyama, *J. Catal.*, 2005, **232**, 85.
- 12.Y. Lei, F. Mehmood, S. Lee, J. Greeley, B. Lee, S. Seifert, R. E. Winans, J. W. Elam, R. J. Meyer, P. C. Redfern, D. Teschner, R. Schlögl, M. J. Pellin, L. A. Curtiss and S. Vajda, *Science*, 2010, **328**, 224.
- 13.P. Wang, Z. Wang, J. Li, Y. Bai, *Microporous Mesoporous Mater.*, 2008, **116**, 400.
- 14.A. B. Castle, E. Gracia-Espino, C. Nieto-Delgado, H. Terrones, M. Terrones and S. Hussain, *ACS Nano*, 2011, **5**, 2458.
- 15.S. E. Davis, M. S. Ide and R. J. Davis, *Green Chem.*, 2013, **15**, 17.
- 16.R. Grabowski, J. Stoczyński, M. Śliwa, D. Mucha, R. P. Socha, M. Lachowska and J. Skrzypek, *ACS Catal.*, 2011, **1**, 266.
- 17.Y. Kobayashi, V. Salgueiriño-Maceira and L. M. Liz-Marzán, *Chem. Mater.*, 2001, **13**, 1630.
- 18.M. Epifani, C. Giannini, L. Tapfer and L. Vasanelli, *J. Am. Ceram. Soc.*, 2000, **83**, 2385.
- 19.X. Ye, Y. Zhou, J. Chen and Y. Sun, *Appl. Surf. Sci.*, 2007, **253**, 6264.
- 20.Y. Sun, *Chem. Soc. Rev.*, 2013, **42**, 2497.
- 21.J. H. Han, S. Lee and J. Cheon, *Chem. Soc. Rev.*, 2013,**42**, 258.
- 22.K. S. Novoselov, A. K. Geim, S. V. Morozov, D. Jiang, Y. Zhang, S. V. Dubonos, I. V. Grigorieva and A. A. Firsov, *Science*, 2004, **306**, 666.
- 23.S. Ghosh, S. S. Acharyya, T. Sasaki and R. Bal. *Green Chem.*, 2015, **17**, 1867.
- 24.S. Ghosh, S. S. Acharyya, R. Tiwari, B. Sarkar, R. K. Singha, C. Pendem, T. Sasaki, and R. Bal, *ACS Catal.*, 2014, **4**, 2169.
- 25.S. S. Acharyya, S. Ghosh and R. Bal, *Chem Commun.*, 2015, **51**, 5998.
- 26.A. Katrizky, J. M. Lagowski, "Chemistry of Heterocyclic N-oxides", Academic Press, London, 1971.
27. A. Albini, *Synthesis*, 1993, 23.
- 28.S.Y Rhie, E. K. Ryu, *Heterocycles*, 1995, **41**,323.
- 29.M. Mac Coss, E. K. Ryu, R. S. White, *J. Org. Chem.*, 1980, **45**, 788.
- 30.A. Albini, S. Pietra, "Heterocyclic N-oxides", CRC Press, Boca Baton, 1991.
- 31.E. Ochiai, O. Aki, T. Morimoto, T. Okata, T. Kaneko, *Tetrahedron Lett.*, 1972,2345.
- 32.C. J. O'Connor, E. Siun, R. L. Carlin, *Inorg. Chem.*, 1977, **16**, 3314.
- 33.(a) A. C. Cope, E. Ciganek., *Org. Synth. Coll. Vol.*, 1963, **4**, 612. (b) P. C. Bulman Page, A. E. Graham, D. Bethell and B. Kevin Park, *Synth. Commun.*, 1993, **23**, 1507.
- 34.Kirk-Othmer, *Encyclopedia of Chemical Technology*, John Wiley and Sons, Wiley-Interscience, New York, 4th edn., 1997, Vol. 23, p. 524.
- 35.T. A. Isbell, T. PAbbott, J. A. Dworak, US Patent 6,051,214, 2000.
36. M. F. Dennis, K. I. Priyadarshini, M. A. Naylor, M. R. L. Stratford and P. J. Wardman, *J. Am. Chem. Soc.* 1996, **118**, 5648.
- 37.V. Boekelheide and W. J. Linn, *J. Am.Chem. Soc.*, 1954, **76**, 1286.
- 38.E. C. Taylor and A. J. Crovetti, *Org. Synth. Coll. Vol.*, 1963, **4**, 828.
- 39.P. Brougham, M. S. Copper, D. A. Cummerson, H. Heaney, N. Thompson, *Synthesis*, 1987, 1015.
- 40.R. W. Murray and R. Jeyaraman, *J. Org. Chem.*, 1985, **50**, 2847.
- 41.M. Ferrer, F. Sanchez-Baeza and A. Messegueur, *Tetrahedron*, 1997, **53**, 1587.
- 42.I. A. O'Neil, A. J. Porter, J. V. Barkley, *Chem. Commun.*, 1998, 251.
- 43.A. Arnone, P. Metrangolo, B. Novo and G. Resnati, *Tetrahedron*, 1998, **54**, 7831.
- 44.H. S. Mosher, L. Turner and A. Carlsmith, *Org. Synth.*, 1963, Coll. 4, 828.
- 45.A. Mc Killop and D. Kemp, *Tetrahedron*, 1983, **45**, 3299.
- 46.B. Meunier, *Chem. Rev.*, 1992, **92**, 1411; (b) B. S. Lane and K. Burgess, *Chem. Rev.*, 2003, **103**, 2457.
- 47.(a) P. Veerakumar, S. Balakumar, and S. Rajagopal, M. Velayudham, *Catal. Sci. Technol.*, 2012, **2**, 1140. (b) M. Gopiraman, H. Bang, S. G. Babu, K. Wei, R. Karvembu and I. S. Kim, *Catal. Sci. Technol.*, 2014, **4**, 2099.
- 48.Y. Ding, W. Zhao, W. Song, Z. Zhang, B. Ma, *Green Chem.*, 2011, **13**, 1486.
49. C. Coperet, H. Adolfsson, T.-A. V. Khuong, A. K. Yudin, K. B. Sharpless, *J. Org. Chem.* 1998, **63**, 1740.
50. A. Thellend, P. Battioni, W. Sanderson, D. Mansuy, *Synthesis* 1997, 1387.
51. K. Bergstad, J. E. Backvall, *J. Org. Chem.* 1998, **63**, 6650.
- 52.H. Masashi, H. Hirotoishi, (Sumitomo Chemical Co., Ltd), Japanese Patent JP 2004307473, 2004;
53. A. J. Bailey, W. P. Griffith, B. C. Parkin, *J. Chem. Soc. Dalton Trans.* 1995, 1833.
54. L. Franz, L. Andre, D. Paul, European Patent EP 224662, 1986.
- 55.L. Rout, T. Punniyamurthy, *Adv. Synth. Catal.* 2005, **347**, 1958.
- 56.D. Limnios and C. G. Kokotos, *Chem. Eur. J.* 2014, **20**, 559.
- 57.K. Neimann and R. Neumann, *Chem. Commun.*, 2001, 487.
- 58.J. Ma, J. Zhang, S. Wang, T. Wang, J. Lian, X. Duan and W. Zheng, *J. Phys. Chem. C*, 2011, **115**, 18157.
- 59.S. E. Lohse, N. D. Burrows, L. Scarabelli, L. M. Liz-Marzán and C. J. Murphy, *Chem Mater.*, 2014, **26**, 34.
- 60.O. Yayapao, T. Thongtem, A. Phuruangrat and S. Thongtem, *J. Alloys Compd.*, 2011, **509**, 2294.
- 61.S. S. Acharyya, S. Ghosh and R. Bal, *ACS Appl. Mater. Interfaces*, 2014, **6**, 14451.
- 62.J. Yu, H. Tao and B. Cheng, *ChemPhysChem*, 2010, **11**, 1617–1618.
- 63.K. Kamata, K. Yonehara, Y. Sumida, K. Hirata, S. Nojima, and N. Mizuno, *Angew. Chem. Int. Ed.*, 2011, **50**, 12062.
- 64.J. C. Chen, R. Y. Zhang, L. Han, B. Tu and D. Y. Zhao, *Nano Res.*, 2013, **6**, 871.
- 65.Q. Fu, W. Li, Y. Yao, H. Liu, H. Su, D. Ma, X. Gu, L. Chen, Z. Wang, H. Zhang, B. Wang and X. Bao, *Science*, 2010, **328**, 1141.

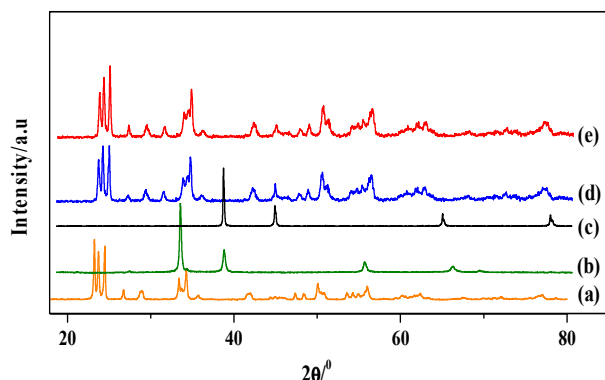


Fig. 1 XRD patterns of a) W (VI) Oxide, b) Ag (I) oxide, c), Ag (0), d) fresh Ag/WO₃ and e) spent Ag/WO₃.

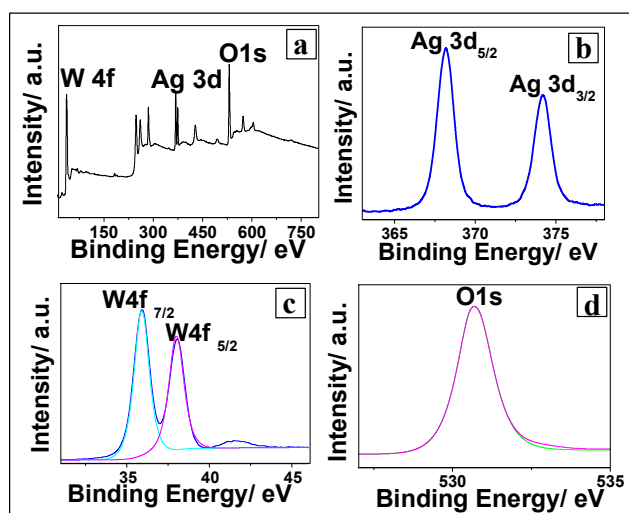


Fig. 2. a) XPS survey spectrum of Ag/WO₃ fresh catalyst, b) Ag 3d, c) W 4f and d) O 1s.

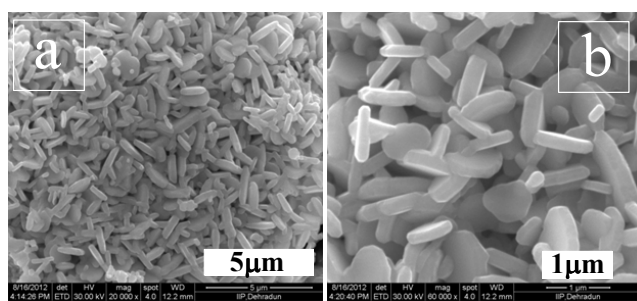


Fig. 3. (a), (b) SEM images of Ag/WO₃ nanoplate catalyst.

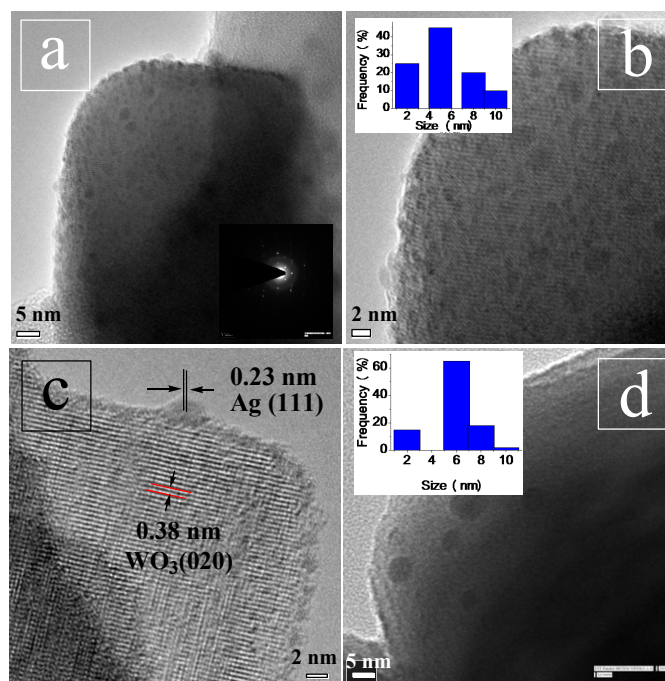


Fig. 4. (a), (b) TEM image of fresh Ag/WO₃ nanostructure catalyst (inset Ag particle size distribution), (c) selected area electron diffraction image (d) lattice fringes and (e), and f) TEM image of used catalyst inset Ag particle size distribution.

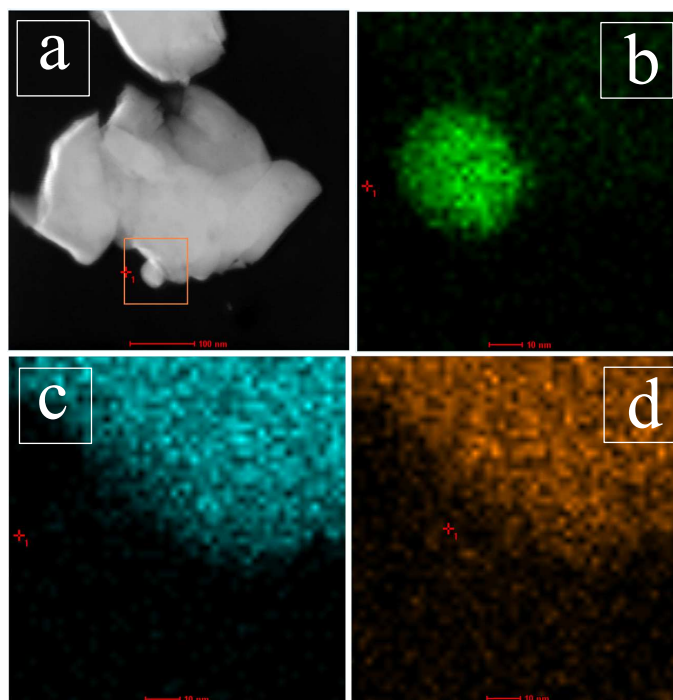


Fig. 5. TEM elemental mapping of Ag/WO₃ catalyst a) TEM image, b) position of silver, c) position of oxygen and d) position of tungsten.

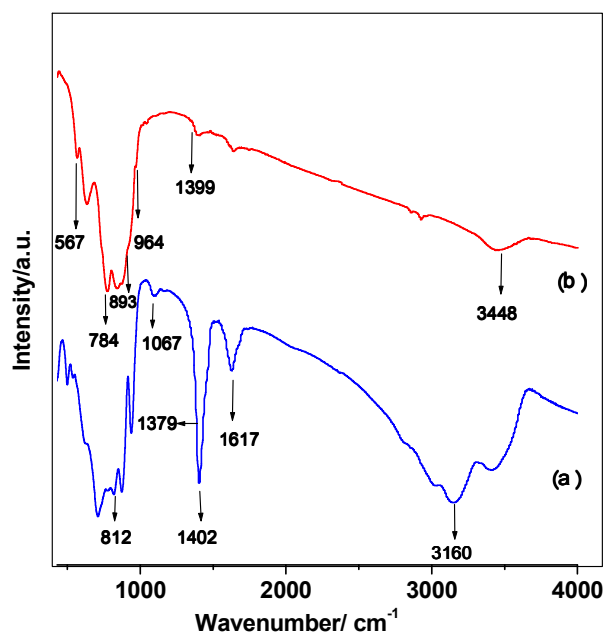


Fig. 6. FTIR analyses of a) uncalcined Ag/WO₃ catalyst, b) calcined Ag/WO₃ catalyst.

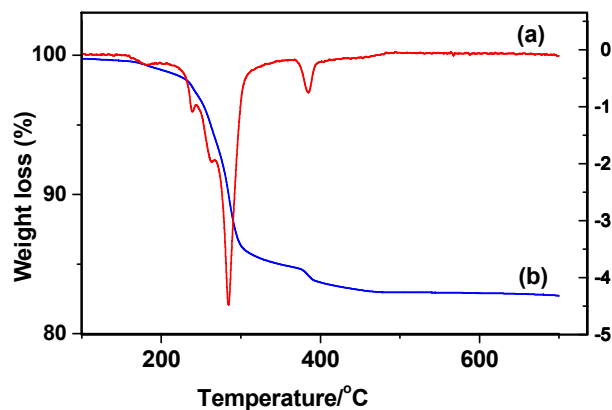


Fig. 7. a) TG and b) DTG analyses of uncalcined Ag/WO₃ catalyst.

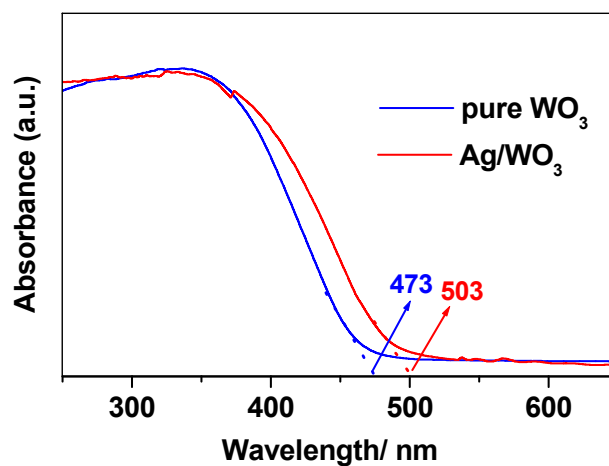


Fig. 8. UV-vis spectra.

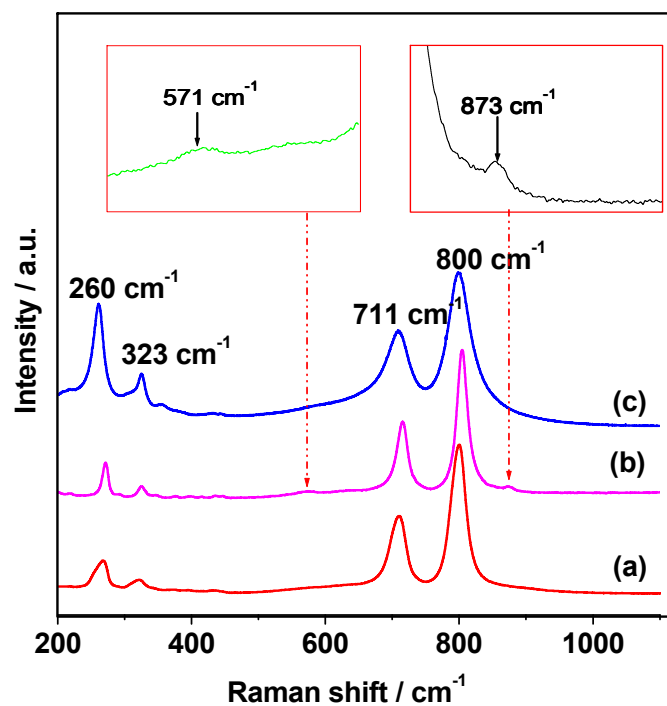


Fig. 9. Raman spectra Ag/WO₃ catalyst a) Fresh catalyst b) Immediate after addition of H₂O₂, c) Spent catalyst.

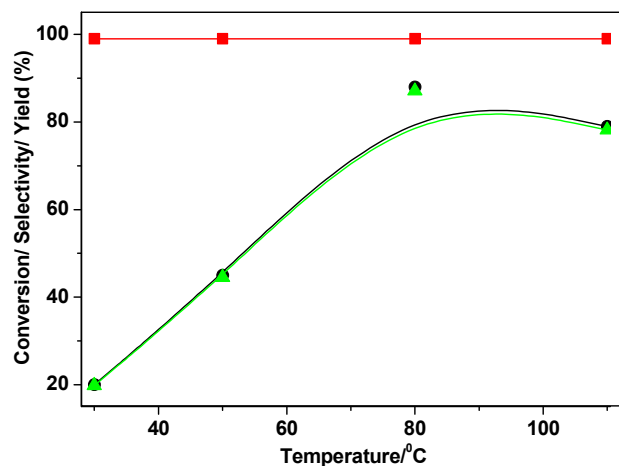


Fig. 10. Effect of temperature on N-oxidation of pyridine.

[■] Conversion of pyridine; [●] Selectivity to pyridine N-oxide; [▲] Yield.

Reaction Condition: Solvent= acetonitrile; Catalyst =0.1g; pyridine:H₂O₂ mole ratio=1:3; Time=24 h.

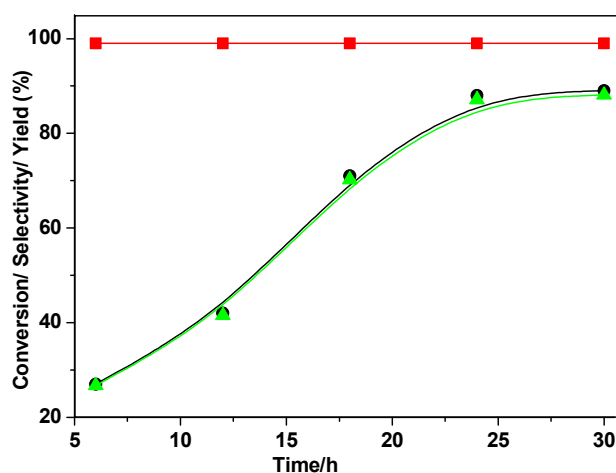


Fig. 12. Effect of time on N-oxidation of pyridine.

[■] Conversion of pyridine; [●] Selectivity to pyridine N-oxide; [▲] Yield.

Reaction Condition: Solvent= acetonitrile; Catalyst =0.1g; Temperature=80°C; pyridine:H₂O₂ mole ratio=1:3.

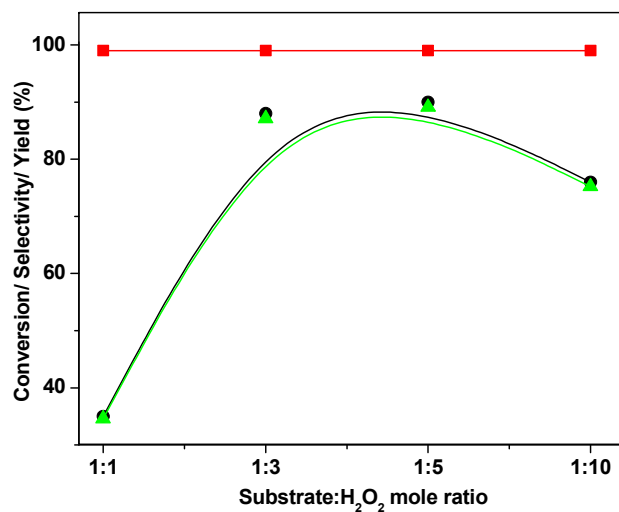
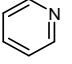
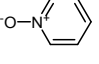
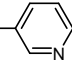
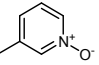
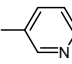
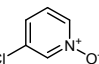
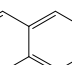
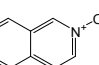
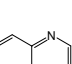
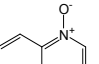
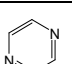
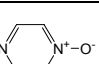
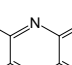
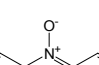


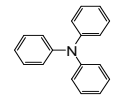
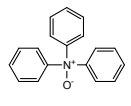
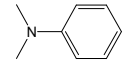
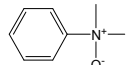
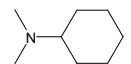
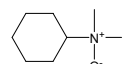
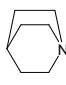
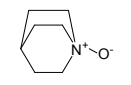
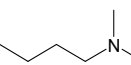
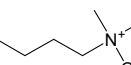
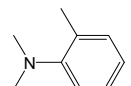
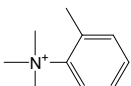
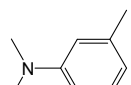
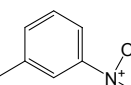
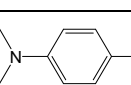
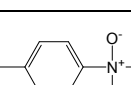
Fig. 11. Effect of substrate: H₂O₂ mole ratio on N-oxidation of pyridine.

[■] Conversion of pyridine; [●] Selectivity to pyridine N-oxide; [▲] Yield.

Reaction Condition: Solvent=acetonitrile; Temperature = 80 °C; Catalyst = 0.1g; Time= 24 h.

Table 1. Oxidation of various substrates catalyzed by Ag/WO₃^a

En try	Sub	C _s ^b (%)	Product	S _p ^c (%)	Y _A ^d (Y _N) (%)
1		88		99	87.1(85.2)
2		92		99	91.0(90.1)
3		90		99	89.1(87.2)
4		87		99	86.1(85.3)
5		92		99	91.0(89.2)
6		91		99	90.0(88.5)
7		91		99	90.0(88.6)

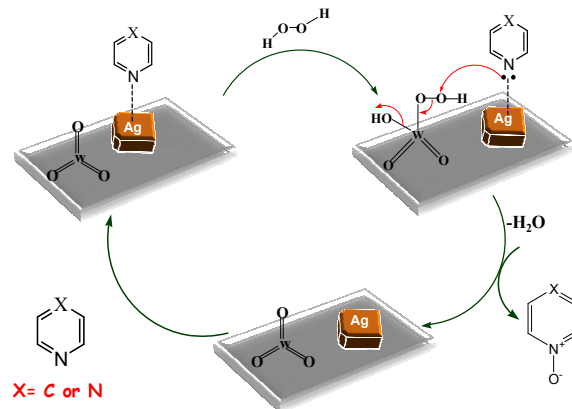
8		85		99	84.1(83.5)
9		87		95	82.6(81.1)
10		72		99	71.2(69.8)
11		61		99	60.3(60.7)
12		64		99	63.3(61.7)
13		85		93	79.0(79.6)
14		89		95	84.5(83.1)
15		88		95	83.6(81.2)

^a Reaction conditions: solvent (acetonitrile) = 10 ml, substrate = 1g, AgWO₃ nanoplate catalyst = 0.10 g, Ag loading= 4.2 wt %; substrate: H₂O₂ mole ratio = 1: 3; Temp = 80° C; time= 24 h; ^bC_T: conversion of substrates ^cSp: selectivity of pyridine oxide; ^dY_A= yield; ^eY_N= isolated yield (parenthesis).

9	Ag/WO ₃ ^g	17	23	3.9	1.3
10	Ag/WO ₃ ^h	-	-	-	-
11	Ag/Cr ₂ O ₃	-	-	-	-
12	Ag/MoO ₃	12	34	4.1	1.36
13	Ag/TiO ₂	-	-	-	-
14	No Catalyst	-	-	-	-

^a Reaction conditions: solvent (acetonitrile) = 10 ml, pyridine = 1g, catalyst weight = 0.10 g, Ag loading= 4.2 wt %; substrate: H₂O₂ mole ratio = 1: 3; Temp = 80° C; time= 24 h; ^bC_T: conversion of substrates ^cSp: selectivity of pyridine oxide; ^dE_o = H₂O₂ efficiency; ^eAg nanoparticles supported on WO₃; ^fcatalyst after 4 reuses; ^gAg/WO₃ catalyst when treated in presence of TBHP; ^hAg/WO₃ catalyst when treated in presence of O₂; Com= Commercial; us= catalyst prepared by surfactant; imp = impregnation method, NP= nanoparticle.

Scheme 1. Plausible reaction mechanism

Table 2 Comparative study of N-oxidation of pyridine based on different catalytic systems^a

Entry	Catalyst	C _T ^b (%)	Sp ^c (%)	Y _A ^d (%)	E _o ^d (%)
1 ^e	Ag ^{com}	2	-	-	-
2 ^f	WO ₃ ^{com}	4	21	0.84	0.28
3	Ag ^{us}	3	16	0.48	0.16
4	WO ₃ ^{us}	6	23	1.4	0.46
5	Ag/WO ₃ ^{imp}	16	43	6.9	2.3
6	Ag/WO ₃ ^e	88	99	87.1	29.0
7	Ag/WO ₃ ^f	87	99	86.1	28.7
8	Ag/WO ₃ ^{NP}	33	99	32.6	10.8

ARTICLE

Journal Name

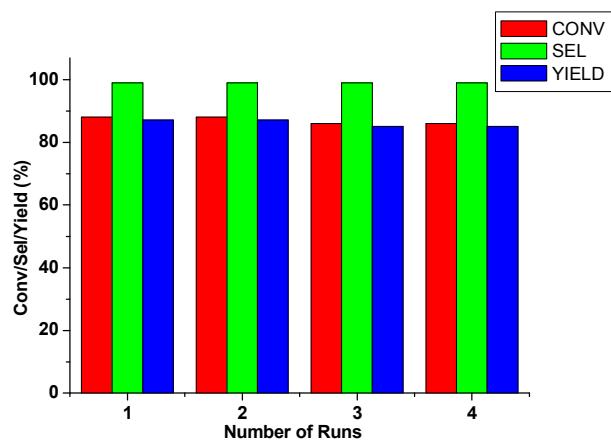


Fig. 13. Reusability test for N-oxidation of pyridine.

Reaction Condition: Solvent= acetonitrile; Catalyst =0.1g;
Temperature=80°C; pyridine:H₂O₂ mole ratio=1:3, time= 24h.